Identification Of Molecular Structures Of Normal And **Pathological Human Breast Tissue Using Synchrotron** Radiation **②**

A. L. C. Conceição; M. E. Poletti AIP Conf. Proc. 1266, 72-77 (2010) https://doi.org/10.1063/1.3478202





Articles You May Be Interested In

Time-resolved small-angle x-ray diffraction from contracting muscle

Konstanz

Rev. Sci. Instrum. (July 1989)

The possibility of using x-ray diffraction with hair to screen for pathologic conditions such as breast cancer AIP Conf. Proc. (February 2000)

SRXRF elemental imaging of a single neuron from patients with neurodegenerative disorders

AIP Conf. Proc. (June 1999)



Identification Of Molecular Structures Of Normal And Pathological Human Breast Tissue Using Synchrotron Radiation

A. L. C. Conceição^{a*} and M. E. Poletti^a

Abstract. Scattering profiles of human breast tissues were measured by x-ray diffraction using a synchrotron radiation source in order to identify their structural features at molecular level $(0.70 \le q \le 70.55 \text{nm}^{-1})$. Several parameters were extracted from these scattering profiles and statistically assessed using discriminant analysis. From this analysis, only the ratio between the peak intensities at $q=19.8 \text{nm}^{-1}$ and at $q=13.9 \text{nm}^{-1}$, as well as the FWHM were statistically significant and allowed distinguishing the human breast tissues with high accuracy, mainly for benign samples where it was found values of sensitivity and specificity of 100%.

Keywords: Breast tissue; x-ray diffraction; synchrotron radiation.

PACS: 34.80.Bm

INTRODUCTION

Breast cancer is the most widespread cancer in women, accounting for more than 1.1 million new cases per year and over than 410 000 die from the disease with the numbers increasing in the last decade [1]. By far the most common diagnostic modality after clinical examination is the mammography; however this technique is able to detect abnormalities only when they are in palpable size. In this sense, several complementary techniques like magnetic resonance imaging, ultrasound, tomosynthesis, phase-contrast imaging and molecular imaging have been introduced in order to try to improve the diagnostic in a early stage, fact that could be provide more chance of cure. On the other hand, it is known that every disease is associated with changes in cell and/or tissue biochemistry with a subsequent effect on the tissue structure [2], fact that sparked a wide interest on investigating of structural features of biological tissues at nanometer scale.

Considering biological samples, it is well-known that the angular distribution of photons scattered by the tissues covering the wide angle regime (scattering profile) is capable of observing changes in molecular tissue structure [2-11] while the small angle regime provides information about supramolecular structures [12-17]. However, a detailed study of the structural properties of the human breast tissues by x-ray

diffraction technique is limited by the low accuracy of the commercial x-ray powder diffractometer [18]. An alternative to this limitation is the use of a synchrotron radiation source, since it has the advantages of present high intensity beam, natural collimation, linear polarization and energy tunability, characteristics that allow time reduction and minimal spectral correction, reducing the experimental uncertainties.

In this paper, we carried out measurements of the scattering profiles of human breast tissues histopathologically classified as normal tissue, benign and malignant lesions using a monoenergetic synchrotron radiation source in order to identify the characteristic structural parameters of each human breast tissue component..

MATERIALS AND METHODS

Breast tissue samples

In this investigation were analyzed a total of 106 human breast samples. Ethical approval was granted the collection of small samples from fresh breast tissues, obtained during mastectomies, biopsies and breast reduction clinical procedures at Hospital das Clínicas da Faculdade de Medicina de Ribeirão Preto, Universidade de São Paulo, Ribeirão Preto, Brazil.

^a Departamento de Física e Matemática, FFCLRP, Universidade de São Paulo, Ribeirão Preto, 14040-901, São Paulo, Brazil

After collection, the samples were stored at room temperature containing formalin (4% formaldehyde in water) in order to preserve the structures within the tissues such as cells walls and nuclei which are needed for accurate histopathological analysis. Just before the measurements, the excess of formalin was withdrawn from the tissues. All considered samples were cut 3mm thick to fit into the circular sample holder with 10mm of diameter and sandwiched between thin mica foils and, after it positioned to carry out the measurements. After measuring, the samples were removed from the sample holder and kept fixed in formalin until they were stained with hematoxylin and eosin to be analysed by a group of breast pathologists for classification of the tissues based on their diagnosis. Three types of breast tissue were histopathologically classified: normal tissue, benign lesion and malignant lesion. However, due to heterogeneity of the normal tissue, it was subdivided into three subgroups: adipose, glandular and peripheral. Peripheral tissue represent those portion excised from patients presenting with a pathology, whose sample was diagnosed as "normal" by the pathologists. The samples division is shown in table 1.

TABLE 1. Histopathology distribution of the human breast samples analyzed in this work.

| Tissue type | Number of samples |
|-------------|-------------------|
| Adipose | 34 |
| Glandular | 7 |
| Peripheral | 26 |
| Benign | 10 |
| Malignant | 29 |

X-ray diffraction experiment

An angular dispersive x-ray diffraction (ADXRD) technique was used in this study. The experiment was carried out at the D12A-XRD1 beam line in the National Synchrotron Light Laboratory (LNLS), Campinas, Brazil [19]. The experimental setup consists basically of a synchrotron light source with an 1.37GeV electron storage ring, delivering approximately 5x10¹⁰ photons.s⁻¹ at 11keV, a mirror to filter photons of high energies and for vertical focusing of the beam, a double-crystal Si (111) monochromator used to provide an x-ray beam energy fixed at 11keV and to reduce the irradiation area on the sample (3.0mm x 1.0 mm) and a Huber three-circle diffractometer operating in transmission mode, where the sample was assembled on a rotative table, 210mm away from the detector. The detector systems consists of a graphite monochromator, which was positioned in order to select only photons scattered with 11keV and to exclude other energies (Compton and multiple scattering), and a fast scintillation detector NaI(Tl) coupled with a monochannel analyzer and controlled by a main computer. Scattering angles from 0.8° to 78.55° were scanned in steps of 0.25° , corresponding to a momentum transfer interval of 0.7nm⁻¹ $\leq q = 4\pi \sin(\theta/2)\lambda^{-1} \leq 70.5$ nm⁻¹, where θ is the scattering angle and λ is the wavelength. An ionization chamber in integrated mode was used to control the incident intensity and to keep the statistical uncertainty less than 2%.

Data handling

All recorder data were submitted to correction and normalization procedures in order to obtain the scattering profile or also called by differential linear coherent scattering coefficient, $\mu_{CS} = n_V (d\sigma/d\Omega)_{CS}$ where n_v is the number of molecules per unit volume and $(d\sigma/d\Omega)_{CS}$ is the coherent molecular differential cross-section [9;20-22]. Firstly, it is needed to remove statistical fluctuations from the scattering distribution data. To do this the acquired data were processed using a zero-phase forward and reverse filter. The second step consists to subtract the number of photons originated from every other spurious scattering sources, which in this case were from three sources: air, mica foils and sample holder, from the measured intensity distribution, I_{M} . This step is summarized below:

$$I_{M_corr} = I_M - \sum_i T_i I_i \tag{2}$$

where I_i represents each spurious sources counting (layer of air, mica foils and bulk sample holder) and T_i the appropriate transmission factor to be applied to each I_i . Additionally, the next step corresponds to corrections due to polarization (P) and sample selfattenuation and geometric effects (A), where both were calculated using standard analytical functions [21;23]. Finally, the last step consists of normalizing the data using a scaling factor K, which is obtained by averaging the ratio between the theoretical data computed within the independent atomic model (IAM) using composition and density values for breast tissues from Woodard and White [24] and the corresponding experimental data correcting by all previous steps, at values, where no interference effects are high expected [6]. For amorphous materials, like breast samples, this approximation is considered valid for $q \ge 50 \, nm^{-1}$. Therefore, the experimental differential linear coherent scattering coefficient is obtained from:

$$\mu_{CS} = KI_{M_corr}(q)P(q)^{-1}A(q)^{-1}$$
 (3)

Statistical Analyses

Parameters definition

After obtaining the scattering profiles, we extracted some parameters from them that represented structural information of each breast tissue type based upon an exploratory data analysis (EDA). For all peaks identified in each scattering profile, parameters like peak intensity, FWHM, and center position were determined for each peak. Another parameter analysed from scattering profiles was the total scattering intensity, which is given by the integration of the scattering profile intensity between $q = 0.70 \text{nm}^{-1}$ and $q = 51.5 \text{nm}^{-1}$, corresponding to the region where the scattering peaks are situated and the groups of breast tissues can be statistically different as described by Cunha *et al.* [7].

Discriminant Analysis

All individual and combined parameters obtained in the EDA approach were considered for the discriminant analysis using a stepwise method with Wilks' lambda as classifying criteria [25]. The SPSS software (Version 13.0, LEAD Technologies, Inc., 2004) was used to verify what these parameters could be statistically significant to differentiate between the groups of breast tissues based on their structural features. The variables identified as significant by Wilks' lambda were used to classify the samples within the groups of tissues and then the sensitivity and specificity of this model were calculated using the leave-one-out cross-validation procedures [7].

RESULTS AND DISCUSSIONS

Breast scattering profiles

The mean scattering profiles of the five groups of breast tissues studied in this work are shown in figure 1 together with the theoretical values for adipose and glandular tissue, obtained assuming IAM and using the atomic-form-factors tabulations of Hubbell et al. [26]. These curves were averaged for all tissues measured within each histological classification and therefore they represent a general characteristic for each type of tissue. In general terms, it is easily seen the scattering profiles as a typical signature of each biological specimen studied, and its behavior present several features strongly dependent on the momentum transfer. Moreover, comparing the experimental and theoretical scattering profiles clear differences are notable, which are due to interference between molecules [11].

In figure 1, the behaviour of the scattering profiles allows identifying structures related to the breast components. Adipose tissue is remarked in the scattering profile by the presence of three peaks. Initially, can be observed a peak at q = 1.38nm⁻¹ only in adipose scattering profile, which is due to the contrast from the packing of triacylglycerides molecules, one of the main constituent of adipose cells (adipocytes) [17]. As increasing the momentum transfer, a peak is identified at q=2.74nm⁻¹ which appear in adipose and peripheral scattering profiles, and this suggests that it can be attributed to a second order harmonic peak of the triacylglycerides packing. Finally, the last adipose peak arises at q=13.9nm⁻¹ and corresponding to interference between fatty acids molecules [4;6;8-10] which binding with glycerides molecules yield triacylglycerides molecules. Yet in figure 1, other two other peaks are clearly visible in glandular, benign and malignant scattering profiles, although differences in the peak heights for each tissue type, being one peak at q=4.1nm⁻¹ related to some component of the extracellular matrix [27] and another well-know peak at q=19.8nm⁻¹ given by the occurrence of the interference between water molecules [4;6], the major component of glandular tissue [24].

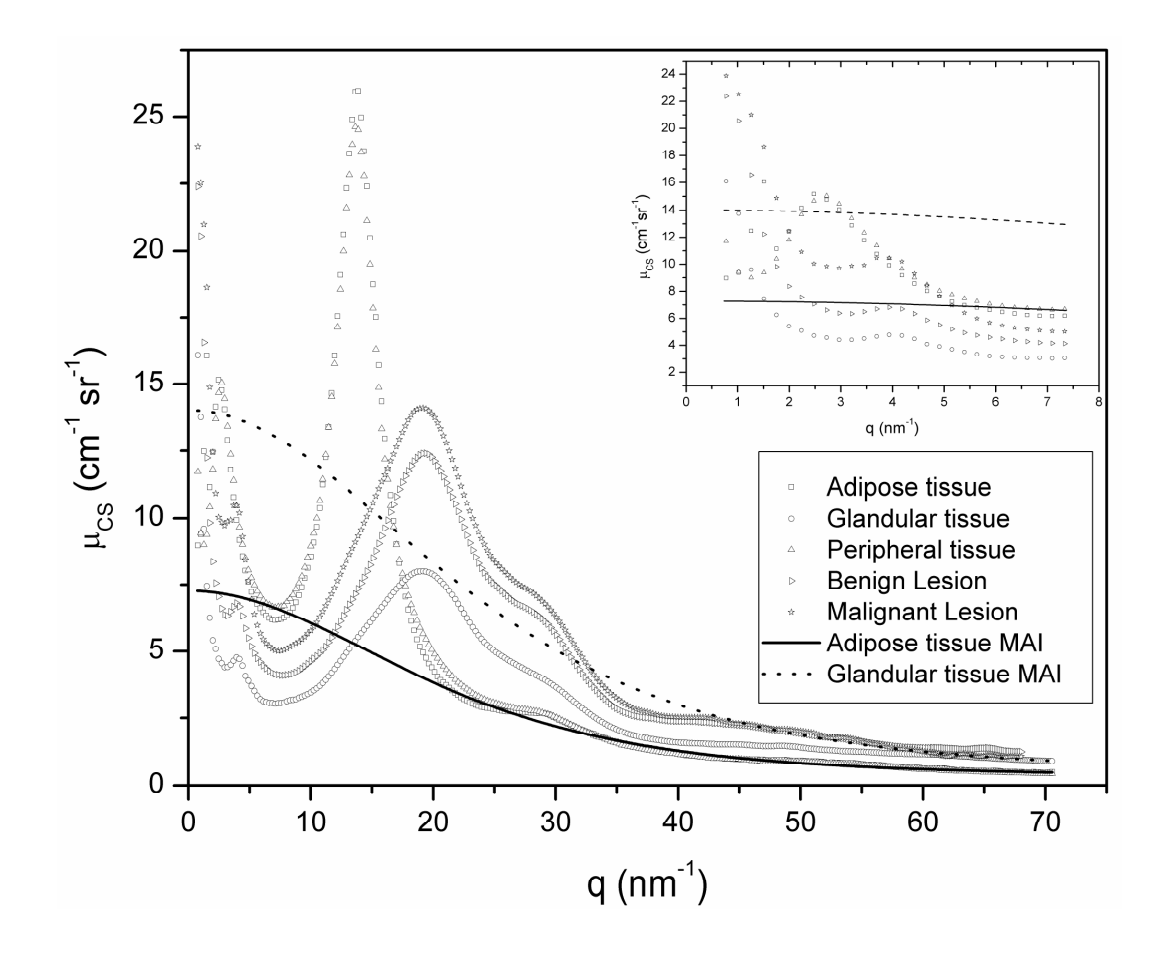


FIGURE 1. Scattering profile of each breast tissue type together with the theoretical values for adipose and glandular tissue.

The scattering profiles of some unusual breast pathologies are shown in figure 2. In figure 2.a is representing the scattering profile of a benign lesion called by adenosis, whose its main feature is an excessive growth of the acins cells [28] and then, its behaviour is very similar to that benign scattering profile exhibited in figure 1, presenting the same two peaks (at q=4.1nm⁻¹ and at q =19.8nm⁻¹). The figure 2.b shows an example of a malignant phyllodes tumour, characterized by a overgrowth of stroma at the expense of the epithelium [28] and its profile seems to that malignant tissue, but the peak at q=19.8nm⁻¹ is more intense. Two cases of ductal carcinoma are representing in figures 2.c and 2.d, comedo and noncomedo type, respectively. The comedo type is more aggressive and, by this reason it presents features like

those of typical malignant scattering profile, while in the scattering profile of non-comedo condition can be noted the presence of a normal component (q=13.9nm⁻¹). Finally, in figure 2.e and 2.f are exhibited the scattering profiles of two particular samples of invasive ductal carcinoma (IDC). Although mucinous carcinoma, figure 2.e, to be a malignant lesion its scattering profile is similar to an adipose profile, which may be related to its main component, mainly mucous [28]. Whereas the figure 2.f shows a case of IDC where it was identified a sharp peak at q=16.7nm⁻¹ which can be due to constructive scattering of crystals of hydroxyapatite, a indicative of the presence of calcification [29].

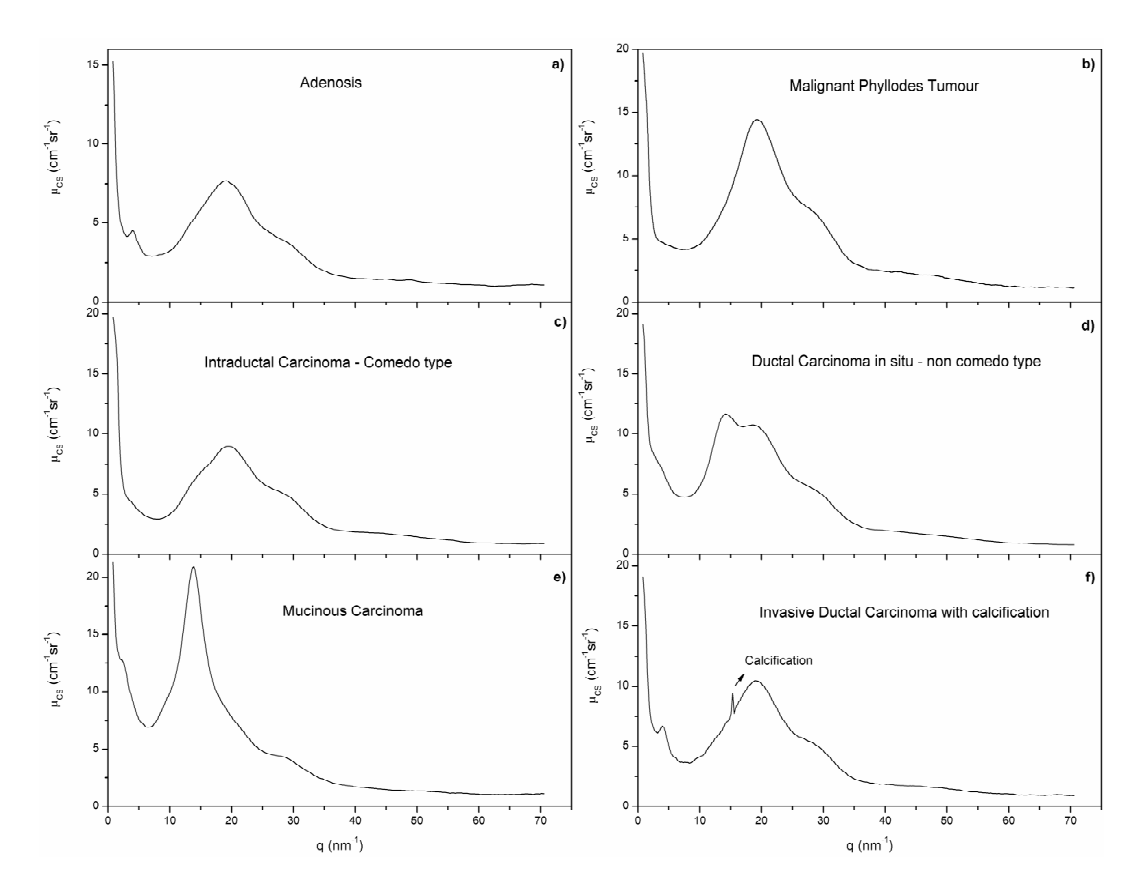


FIGURE 2. Unusual types of breast pathologies. 2.a) is a benign condition called by adenosis, while the other five types are malignant: 2.b) phyllodes tumour; 2.c) intraductal carcinoma – comedo type; 2.d) ductal carcinoma in situ – non-comedo type; 2.e) mucinous carcinoma and 2.f) invasive ductal carcinoma presenting calcification.

Breast tissue classification

Regarding the five characteristic peaks of the breast components structures at the momentum transfer analyzed in this work, the individual parameters obtained in the EDA approach were statistically assessed together with new features originated from combinations between these individual parameters. From the discriminant analysis only the ratio between the peak intensities at q=19.8nm⁻¹ and q=13.9nm⁻¹ and the FWHM were statistically significant (p<0.001), these two parameters were plotted one against other and the figure 3 shows the spatial distribution of the breast samples. From figure 3, it is clear that benign samples are always distinguished from the other tissue types. Yet, the normal samples present into the malignant lesion region are those classified as glandular tissue, while the malignant samples present into normal region are due to mucinous carcinoma. Then, the values of these two classifiers were submitted to a cross-validation procedure and the results of sensitivity and specificity for each group of breast tissue are shown in table 2.

With basis on table 2, high values of sensitivity and specificity are observed for all groups, except for the sensitivity of malignant tissue, what can be due to the heterogeneity of the breast cancer samples. Although the values of sensitivity are not so high in order to differentiate normal and malignant tissues, this approach fills a lack in the field of breast cancer diagnosis, since it allows differentiating correctly the benign samples from the other tissues.

TABLE 2. Performance of the breast tissue diagnostic model.

| Tissue Comparisons | Sensitivity (%) | Specificity (%) |
|------------------------|-----------------|-----------------|
| Normal vs Benign | 100 | 100 |
| Normal vs Malignant | 79 | 96 |
| Benign vs Malignant | 100 | 99 |

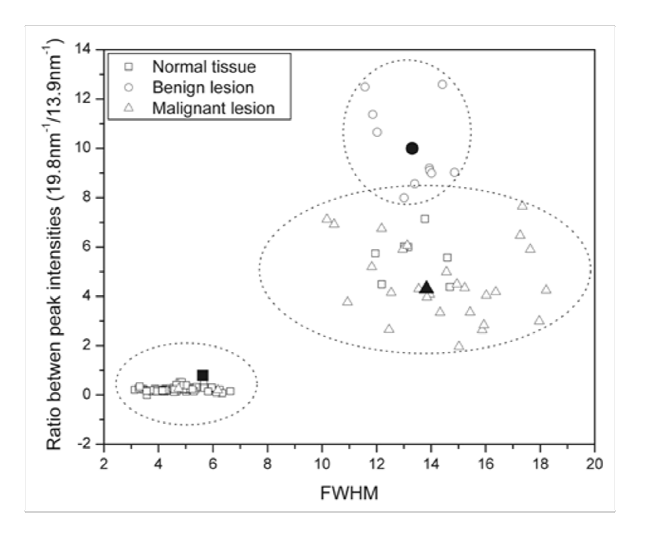


FIGURE 3. Sample distribution on basis combining the ratio between peak intensities at q=19.8nm⁻¹ and q=13.9nm⁻¹ and the FWHM.

CONCLUSION

In this work, x-ray diffraction technique using synchrotron radiation was applied to human breast tissues in order to determine the structures of their components. The analysis of the scattering profiles of all groups of tissues allows identify peaks that represent features of structural and functional breast components. From statistical assessment of the scattering profiles it was possible identify that the ratio between the peak intensities at q=19.8nm⁻¹ and q=13.9nm⁻¹ and the FWHM were potentials breast tissue classifiers, differentiating benign tissues from normal and malignant tissues with a sensitivity and a specificity of 100%. These results encourage us to pursue further studies in order to improve this approach by combining it with the results of another technique.

ACKNOWLEDGMENTS

The authors would like to acknowledge the support by the Brazilian agencies Fundação de Amparo à Pesquisa do Estado de São Paulo (FAPESP) and Conselho Nacional de Desenvolvimento Científico e Tecnológico (CNPq), as well as the D12A-XRD1 beam lines staff for the help during the experiments in the National Synchrotron Light Laboratory (LNLS). In addition, we also would like to thank the Departmento de Patologia do Hospital das Clínicas, Faculdade de Medicina de Ribeirão Preto, Brazil, for it allows the human breast samples collection.

REFERENCES

- J. Ferlay, F. Bray, et al. GLOBOCAN 2002: Cancer Incidence Mortality and Prevalence. Worldwide IARC Cancer Base No. 5 version 2.0 (Lyon: IARC Press) (2004).
- A. A. Vazina, et al. Nucl. Instr. and Meth. A 543 297-301 (2005).
- 3. S.H. Evans, et al. Phys. Med. Biol. 36 7-18 (1991).
- 4. G. Kidane, et al. Phys. Med. Biol. 44 1791-1802 (1999).
- 5. R. Speller. X-Ray Spectrom. 28 244-250 (1999).
- 6. M.E. Poletti, et al. Phys. Med. Biol. 47 47-63 (2002).
- 7. D.M. Cunha, et al. X-Ray Spectrom. 35 370-374 (2006).
- 8. J. A. Griffiths, et al. Phys. Med. Biol. **52**, 6151-6164 (2007)
- 9. O.R. Oliveira, et al., J. Radiat. Res. 49 527-532 (2008).
- A. L. C. Conceição, et al. Appl. Radiat. Isot. 68 799-803 (2010).
- A. L. C. Conceição, et al. Nucl. Instr. and Meth. A. In press; doi:10.1016/j.nima.2009.12.021.
- 12. R. A. Lewis, et al. J. Synchrotron Rad. 7 348-352
- 13. M. Fernández, et al. Phys. Med. Biol. 47 577-592 (2002).
- 14. A. R. Round, et. al. Phys. Med. Biol. **50** 4159-4168 (2005).
- 15. G. Falzon, et al. Phys. Med. Biol. 51 2465-2477 (2006).
- 16. S. Sidhu, et al. Med. Phys. 35 4660-4670 (2008).
- 17. A.L.C. Conceição, et al. Analyst, 134 1077-1082 (2009).
- 18. P.C. Johns and M.P. Wismayer, *Phys. Med. Biol.* **49** 5233-5250 (2004).
- 19. C. Cusatis, et al. J. Synchrotron Rad. 5 491-493 (1998).
- 20. J. Kosanetzky, et al. Med. Phys. 14 526-532 (1987).
- M.E. Poletti, et al. Nucl. Instr. and Meth. B 187 437-446 (2002).
- 22. A. Tartari, et al. Appl. Radiat. Isot. 49 631-633 (1998).
- 23. O.D. Gonçalves and S.D. Magalhães. *Radiat. Phys. Chem.* **59** 201-209 (2000).
- H.Q. Woodard and D.R. White. Br. J. Radiol. 59 1209-1218 (1986).
- B. S. Everitt and G. Dunn, in Applied Multivariate Data Analysis, ed. Edward Arnold, Arnold Publication, London, 2nd edn., 2001, pp. 219-220.
- J.H. Hubbell and I. Øverbø, J. Phys. Chem. Ref. Data 8 69- (1979).
- 27. S. Bouyain, et al. PNAS, 102 15024 (2005).
- 28. Lazlo Tabar. Pathology reporting of breast disease. Guidelines for Pathology Reporting in Breast Cancer Screening. 2005.
- M. J. Farquharson and R. D. Speller. *J. Archaeolog. Sc.*. 24 765-772 (1997).